Robotica (2008) volume 26, pp. 655–665. © 2008 Cambridge University Press
doi:10.1017/S026357470800427X Printed in the United Kingdom

Vibration control of elastodynamic response of a 3-PRR flexible parallel manipulator using PZT transducers

Xuping Zhang*, James K. Mills and William L. Cleghorn

Department of Mechanical and Industrial Engineering, University of Toronto 5 King's College Road, Toronto, Ontario, Canada, M5S 3G8

(Received in Final Form: February 7, 2008. First published online: March 27, 2008)

SUMMARY

This paper addresses the dynamic simulation and control of structural vibrations of a 3-PRR parallel manipulator with three flexible intermediate links, to which are bonded lead zirconate titanate (PZT) actuators and sensors. Flexible intermediate links are modelled as Euler–Bernoulli beams with pinned-pinned boundary conditions. A PZT actuator controller is designed based on strain rate **feedback** (SRF) control. Control moments from PZT actuators are transformed to force vectors in modal space and are incorporated in the dynamic model of the manipulator. The dynamic equations are developed based on the assumed mode method for the flexible parallel manipulator with multiple PZT actuator and sensor patches. Numerical simulation is performed and the results indicate that the proposed active vibration control strategy is effective. Spectral analyses of structural vibrations further illustrate that deformations from structural vibration of flexible links are suppressed to a significant extent when the proposed vibration control strategy is employed, while the deflections caused by inertial and coupling forces are not reduced.

KEYWORDS: Flexible manipulators; Parallel manipulators; Assumed mode; Strain rate feedback; PZT Transducers.

1. Introduction

The use of parallel robot manipulators has increased in various manufacturing industries such as precision optics, nano-manipulation, and medical surgery, due to the advantages of parallel link manipulators over serial link manipulators. These advantages include higher strength-to-weight and stiffness-to-weight ratios and higher accuracy. On the other hand, the motion task requirements of high speed and high acceleration require industrial robot manipulators to be designed and constructed with light weight links which are capable of moving swiftly. Light weight manipulators offer advantages including higher speed, lower energy usage, improved mobility, and higher payload-to-arm weight ratio. In light of these advantages, a planar parallel manipulator with light weight links is developed to provide an alternative high-speed pick-and-place positioning mechanism to serial architecture manipulators, i.e., X–Y tables or gantry robots, designed for electronic manufacturing. The parallel manipulator presented in this work, and shown in Fig. 1, is categorized as a 3-PRR type because it has three symmetric closed-loop chains, each of which consists of a prismatic joint (P) and two consecutive revolute joints (R). Due to its inherently greater stiffness and accuracy, coupled with the low inertia of moving links, this proposed mechanism can be used in high-speed and high-accuracy robotic applications such as a planar positioning and orientating device [36]. While light weight links are used to better meet the demands of high speed and high acceleration placement, such light weight links are more likely to deflect and vibrate due to the inertial forces and external forces such as those arising from actuators. Structural flexibility effects are much more pronounced at high operational speeds and accelerations of the end-effector.

To address these concerns, here we first develop a dynamic model of the 3-PRR manipulator to investigate the dynamic characteristics of these structural vibrations. Subsequently, we develop an effective vibration control methodology to suppress these unwanted structural vibrations during high speed and acceleration of the parallel robot. Utilizing simulation tools, the dynamic behavior of rigid body motion and structural flexibility of the linkages of the planar parallel manipulator has been thoroughly investigated.

The dynamic model formulation of flexible linkage manipulators and mechanisms has been investigated extensively, with dynamic based on the finite element method (FEM)[1,2] and the assumed mode method (AMM).[3,4] Early investigations mainly involved the dynamic modelling of flexible serial manipulators and four-bar mechanisms, with detailed reviews of this work found in ref. [5]. While substantial work has been reported on the dynamic modelling of flexible serial manipulators and four-bar mechanisms, less work has been reported on the dynamic modelling of parallel manipulators,[30] especially for parallel manipulators with flexible links. Recently, a general approach was presented to perform the dynamic analysis of flexible closed-chain manipulators using the principle of virtual work.[6] A dynamic model was developed for a flexible Stewart platform using Lagrange's equations.[7] Dynamic equations of a flexible 3PRS manipulator were established using the FEM.[8] Based on the FEM, a dynamic modelling procedure was developed for a 3-PRR planar parallel manipulator with flexible links.[9] Modal identification tests performed in ref. [10] showed that mode properties of the links match pinned-pinned boundary conditions.

* Corresponding author. E-mail: zhxp@mie.utoronto.ca

https://doi.org/10.1017/S026357470800427X Published online by Cambridge University Press

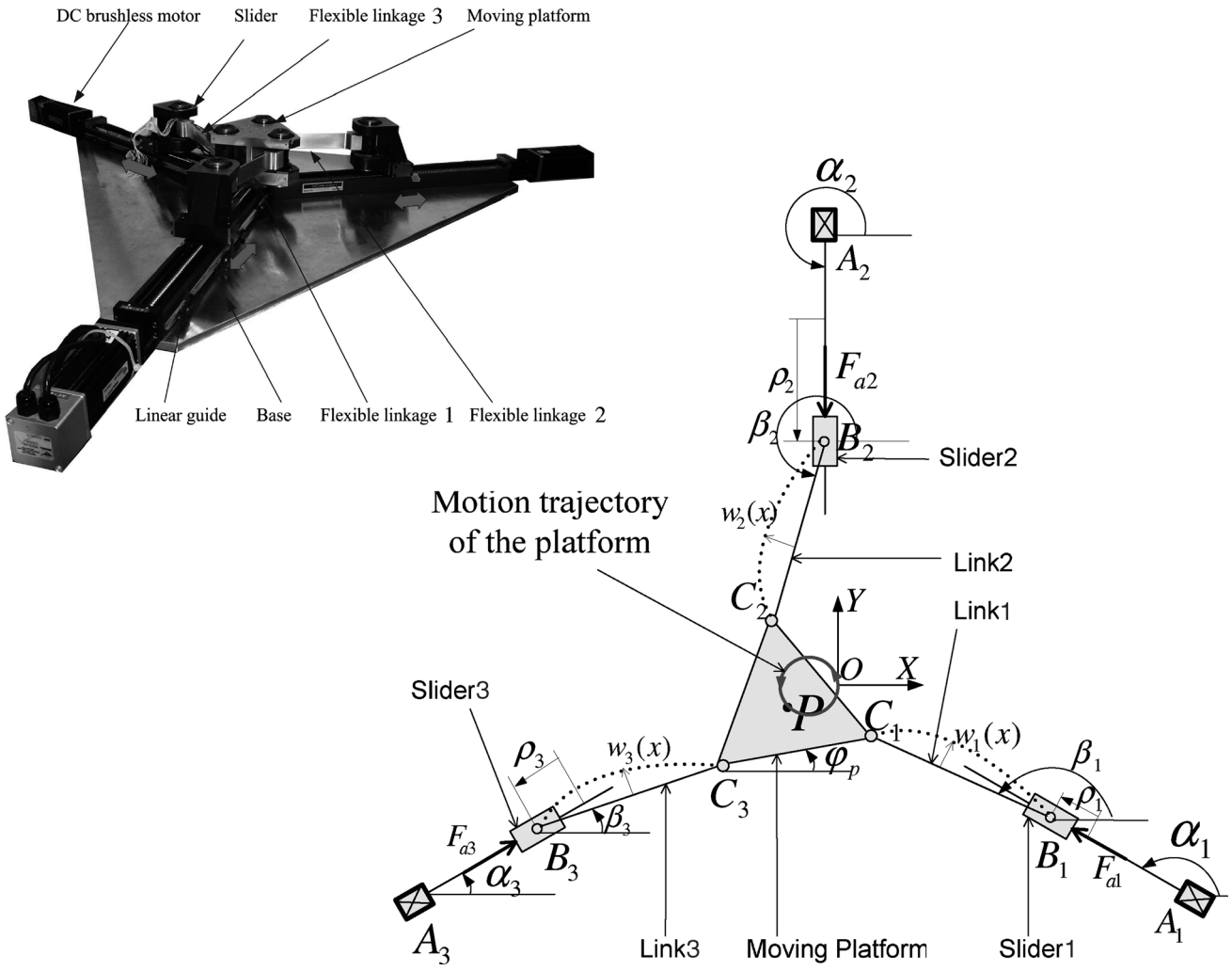


Fig. 1. Architecture and coordinate system of the proposed manipulator.

Concurrent to the work on dynamic modelling as discussed above, investigation of vibration control of flexible manipulators and mechanisms has been undertaken by many researchers. A variety of design or control strategies have been presented to suppress the unwanted vibration of flexible links. For example, refs. [11, 12] optimize the cross-sectional geometry of the flexible links to suppress vibration; refs. [13, 14] use additional damping materials to dissipate the vibration; refs. [15, 16] employ composite materials to construct linkages of mechanisms and manipulators to damp structural vibration. These composite materials have inherently superior damping characteristics and higher stiffness to weight ratios. These above approaches to vibration control are usually referred to as passive vibration control. Work in ref. [17] presents the design of an additional electromechanical actuator, which is integrated into a four-bar mechanism at the proximal end of the follower link, which reduces the deflection of the flexible linkages by controlling the additional actuator. Other method advocates the reduction of linkage structural vibrations through control of joint motions or joint torques based on input shaping,[18] or singular perturbation techniques,[19,31] etc. However, the successful realization of joint motion or torque control schemes may be very difficult to achieve due to hardware limitations such as motor output torque saturation, signal noise from the sensor, and parameter variations. These difficulties may be mitigated by adopting the use of smart materials featuring distributed actuators and sensors fixed to flexible links to control the unwanted vibration.[25,27]

Recently, considerable attention has been focused on the development of technologies associated with "smart" or "intelligent" structures. These smart structures are comprised of sensing, actuating, tuning, controlling, and computing capabilities. These characteristics allow the smart structures to be employed to control the static and elastodynamic response of distributed parameter systems operation under variable service conditions in uncertain environments. Significant progress has been made in the development of smart structures featuring piezoelectric materials, shape memory alloys, and electro-rheological fluids. Smart structures with surface-mounted or embedded piezoelectric materials have received growing attention in vibration control of flexible structures in recent years, due to the favourable properties of piezoelectric actuators and sensors, such as mechanical simplicity, small volume, light weight, large bandwidth, efficient conversion between electrical energy and mechanical energy, and simple integration with various metallic and composite structures. Two types of piezoelectric

https://doi.org/10.1017/S026357470800427X Published online by Cambridge University Press

materials may be used: polyvinylidene fluoride (PVDF),[20–22] and lead zirconate titanate (PZT).[23–28] PZT transducers exhibit a greater capability than PVDF to damp vibrations because their strain constant is roughly five times greater than that of PVDF. Therefore, in this work, smart structures featuring PZT sensors and actuators are employed to suppress unwanted vibrations of the flexible parallel manipulator. Several feedback control techniques have been developed for vibration control, including angular velocity feedback,[21] L-type linear velocity feedback,[28] strain feedback, and strain rate feedback[26] of the controlled points on flexible structures. Other active vibration control strategies in the literature include independent modal space control (IMSC),[32] modified independent modal space control (MIMSC),[33] and efficient modal control (EMC),[34] These modal space control strategies are investigated and compared by Singh *et al*.[34] Strain rate feedback (SRF) has a wider active damping frequency region, and it can stabilize more than one mode simultaneously, given sufficient bandwidth. Moreover, the strain rate is readily available in practice by differentiating the voltages measured from PZT sensors.

The research on active vibration control of flexible structures using piezoelectric actuators and sensors was initiated by Bailey and Hubbard.[21] They proposed simple, but effective control algorithms for transient vibration control. Early investigation in this field mainly involved vibration control of space-based flexible structures. Since the 1990s, piezoelectric actuators and sensors have been introduced for vibration damping of flexible manipulators and mechanisms.[23,25,27] Most of these works investigate the residual vibration control of manipulators and mechanisms with a single flexible link bonded with single actuator and sensor.

This paper addresses the structural vibration control of elastodynamic responses of a 3-PRR parallel manipulator with three flexible intermediate links with multiple PZT actuators and sensors bonded to these links when the manipulator moves with high speed and acceleration. Considering that the AMM is based on the dynamic behavior of the system, i.e., natural frequencies and mode shapes, and the AMM has better computational efficiency compared with the FEM approach, hence the AMM is used to model link flexibility in this work. The intermediate links are modelled as Euler–Bernoulli beams with pinned-pinned boundary conditions. It is assumed that the vibration behavior is excited mainly by the driving forces from actuation motors, the inertial forces, and the reaction due to the payload fixed to the moving platform. The centralized bending moments from the PZT actuators bonded on flexible intermediate links, are transformed to the force vectors in modal space and are incorporated into the dynamic equation of the flexible manipulator. The resultant dynamic equations provide essential insight to the active vibration control of smart structures featuring PZT actuators and sensors. Numerical simulation of the 3-PRR parallel manipulator is performed with three flexible links, and simulation results verify that the proposed active control strategy is effective.

In this simulation, the first three modes are modelled and controlled based on SRF. One PZT pair is bonded to the midpoint of each intermediate link, the high strain location of the first and third vibration modes. However, the midpoint is the node of the second-order vibration mode for each intermediate link. Therefore, the other two pairs are bonded to its quarter points, the high strain locations of the second vibration mode. Although the second-order vibration mode can be suppressed using only one PZT pair bonded to either one of two quarter points of each link, two pairs of actuators can suppress the vibration more effectively with the same voltages applied on PZT actuators. Several approaches have proposed modal space vibration control strategies, such as MIMC and EMC, in which fewer actuators can control several modes.[3,4] However, we note that the required voltages applied to PZT actuators are relatively high, and modal filters are also required if these modal vibration control methods are adopted. Further, the strain rate is readily available in practice through differentiation of the voltages measured from PZT sensors. Therefore, in this simulation, three PZT actuators and sensors are modelled as bonded to each of three flexible links, with the vibration controller design based on RSF. In this work, no rigorous attempt to calculate the optimal number and locations, and control gains has been made by the authors. The ideal number, location of sensors and actuators, and control gains are the complex problems for multiple sensor–actuator pairs and multiple modal vibration controls. These problems can be solved by genetic algorithms or other optimization techniques.[37,38]

Usually, the precise parametric modelling of a multi-link flexible robot is time consuming and problematic to use for real-time control, as precise models are very complex in nature. Here, we neglect the axial deformation and the effect of longitudinal loads on lateral stiffness. Linearization and model order reduction techniques are used to simplify the dynamic equations. The modelling errors and other structured uncertainty are considered as parameter perturbations. While not the subject of this work, adaptive and learning control technologies may be adopted to implement the vibration control of flexible links and joint motion control, to compensate for these uncertainties.

2. Modelling of the Structural Flexibility of an Individual Intermediate Link

In this section, we develop the dynamic model of a 3-PRR planar parallel robot with three flexible linkages to be used for simulation. The structure and coordinate system for the parallel robot modelled here is defined in Fig. 1, with undeformed links shown. This planar parallel manipulator has three symmetric kinematic chains, i.e., $[\alpha_1 \ \alpha_2 \ \alpha_3] = [150^\circ \ 270^\circ \ 30^\circ]$. Variable α_i is the angle at A_i between the X-axis of the fixed frame and the ith linear guide. Each kinematic chain has a P-R-R structure, i.e., an active prismatic joint A_i, followed by two consecutive passive revolute joints B_i and C_i. Each active prismatic joint is implemented at A_i, $i = 1, 2, 3$ with an Aerotech BM200 DC brushless servo motor with peak torque $3.5N \cdot m$ and a ball screw and linear guide mechanism. The ball screw converts the rotation of motors into the translational motion of the slider along the linear guide, i.e., ρ_i, $i = 1, 2, 3$. The origin of ρ_i is selected at the center of each linear guide. Variable F_{ai} is the driving force acted on by the ith slider.

https://doi.org/10.1017/S026357470800427X Published online by Cambridge University Press

Revolute joints collocated with the sliders, at B_i, $i = 1, 2, 3$, connect the slider with intermediate linkages. The other ends of the linkages,C_i, $i = 1, 2, 3$, connect the linkages with the moving platform, which constrains the motion of linkages. The origin of the fixed frame is located at O, which is the center point of the moving platform when $\alpha_i = \beta_i$. Variable β_i is the angle at B_i between the X-axis of the fixed frame and the ith intermediate link. The moving platform, i.e., the end-effector, is of a regular triangle shape ($C_1C_2C_3$), and moves in the plane with three degrees of freedom. The variables x_p, y_p and φ_p are used to denote the position and orientation of the moving platform.

To utilize the AMM, the elastic deflection of intermediate linkages, shown in Fig. 1 with dotted lines, is described by an infinite number of separable harmonic modes. Since the first few modes dominate the dynamics, the modes are truncated to a finite modal series in terms of spatial mode Eigen-functions $\psi_{ij}(x)$ and time-varying mode amplitudes $\eta_{ij}(t)$. Therefore, utilizing the AMM formulation, the lateral flexible deformation of the ith intermediate link can be expressed as,

$$w_i(x,t) = \sum_{j=1}^{r} \eta_{ij}(t)\psi_{ij}(x) \quad i = 1, 2, 3 \tag{1}$$

where w_i is the lateral deformation of the ith intermediate link, the η_{ij} is the jth mode coordinate of the ith intermediate link, and ψ_{ij} is the jth mode shape function of the ith intermediate link, r represents the number of assumed modes.

The platform and sliders are significantly stiffer mechanical structures than the intermediate links, and hence are assumed rigid. Since the mass and stiffness of the attached piezoelectric patches are small in comparison with those of the intermediate links, for simplicity, the effect of this added mass and stiffness is neglected in the dynamic modelling formulation of intermediate links. Each intermediate link can be treated as an Euler–Bernoulli beam because the length of each link is much longer than its thickness. Each intermediate link has rotary joints at its ends connecting to the platform and a slider. The pinned-pinned boundary condition is adopted for the intermediate links based on results in ref. [10], which showed that modal characteristics of the intermediate link match the pinned-pinned boundary condition. From transverse beam vibration theory, position-dependant pinned-pinned mode shape functions $\psi_{ij}(\xi)$ are given as

$$\psi_{ij}(x) = \sin(j\pi x/l_i) = \sin(j\pi\xi) = \psi_{ij}(\xi)$$
$$j = 1, 2, \ldots, r \tag{2}$$

where $\xi = x/l_i$, r is the number of selected assumed modes, x is the distance from the arbitrary point on the ith intermediate link to B_i, and l_i is the length of the ith intermediate link.

Flexible generalized coordinates are defined as

$$\bar{\eta} = [\eta_{11} \ \cdots \ \eta_{1r} \quad \eta_{21} \ \cdots \ \eta_{2r} \quad \eta_{31} \ \cdots \ \eta_{3r}]^T. \tag{3}$$

3. Sensor and Actuator Dynamics based on Strain Rate Feedback Control

PZT materials have the potential to both damp vibrations and measure the vibration characteristics of distributed parameter systems, due to the direct and converse piezoelectric effect. The system is constructed by bonding PZT patches to the two opposite sides of the intermediate link as shown in Fig. 2. The PZT patches on one side of the beam plays the role of actuators, while the PZT patches on the opposite side plays the role of sensors. One actuator and one sensor constitute a PZT control pair, and are located at the same position along the beam.

3.1. Sensor dynamics

Strains are generated in the PZT sensors bonded on the intermediate links due to the lateral vibration of the flexible links. According to the direct piezoelectric effect, the strains in a PZT sensor along the$x$ direction leads to a charge signal on the upper and lower surfaces of the PZT sensor. Integration of the charge signal over the sensor area gives the total amount of charge generated. Considering the fact that PZT sensor dimension along the x direction is very short compared to the length of the beam, the axial strain over a sensor is approximately equal to that of midpoint of the PZT sensor. Using an impedance converter, a charge signal is converted to a voltage signal proportional to the strain at

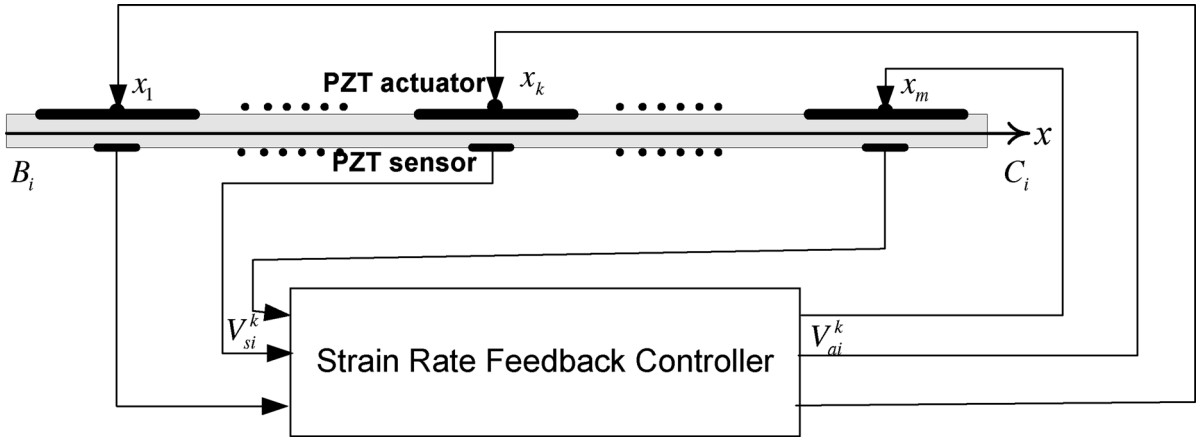


Fig. 2. A smart beam structure with PZT actuator and sensor patches (top view).

https://doi.org/10.1017/S026357470800427X Published online by Cambridge University Press

the midpoint of a sensor. Therefore, the voltage produced by the sensor located at x_k on the ith intermediate link can be expressed by

$$V_{si}^k = k_{si}^k \left(\frac{\partial w_i^2(x_k, t)}{\partial x^2} \right) = k_{si}^k \sum_{j=1}^{r} \eta_{ij}(t) \psi_{ij}^{"}(x_k)$$
$$= \frac{E_p d_{31} w_p}{C_p} (h_p + h_i) \sum_{j=1}^{r} \eta_{ij}(t) \psi_{ij}^{"}(x_k) \quad (4)$$

where k_{si}^k is the sensor constant (V^{-1}), E_p the Young's modulus of PZT materials (N/m^2), d_{31} is the piezoelectric constant ($m \cdot V$), w_p the width of the PZT actuator (m), h_i the height of the link, h_p the height of the PZT actuator (m), and C_p is the capacitance of the sensor (Farad).

3.2. Actuator dynamics

According to the converse piezoelectric effect, applying a voltage on a PZT actuator, strain is produced in the PZT actuator. When a stiff boundary layer is used to bond the actuator to the host structure (one of the intermediate links), the shear strain is transferred between the actuator and the beam over an infinitesimal distance near the ends of the actuator.[24] Therefore, the action resulting from the converse piezoelectric effect is represented by two concentrated bending moments applied at both the ends of the actuator. The bending moments generated by the kth actuator of the ith intermediate links are give as

$$M_{pi}^k(x_{k1}) = -M_{pi}^k(x_{k2})$$
$$= -d_{31} \frac{E_i E_p h_i^2 w_i w_p}{E_i h_i w_i + E_p h_p w_p} V_{ai}^k = -k_{ai}^k V_{ai}^k \quad (5)$$

where E_i is the Young's modulus of the ith link, w_i is the width of the link, and V_{ai}^k is the voltage applied on the PZT actuator, x_{k1} is the coordinate of the left end of the actuator, and x_{k2} is the coordinate of the right end of the actuator.

Using modal theory, the bending moment (expressed in physical space) can be transformed to the force vector in modal space.[27] The modal force vector is given by

$$F_{pi}^k = [\psi_{i1}'(x_{k2}) - \psi_{i1}'(x_{k1}), \cdots, \psi_{ij}'(x_{k2}) - \psi_{ij}'(x_{k1}), \cdots,$$
$$\times \psi_{ir}'(x_{k2}) - \psi_{ir}'(x_{k1})]^T M_{pi}^k(x_{k2}) \quad (6)$$

where "′" denotes the derivative with respect to x.

3.3. Strain rate feedback control

In this work, strain rate feedback control (SRF) is used to damp the lateral vibrations of the flexible intermediate links. Using SRF, the derivative of a voltage from a PZT sensor is multiplied by a negative control gain $-k_{di}^k$ and fed back to the corresponding actuator. Therefore, the voltage applied on the actuator is expressed as

$$V_{ai}^k = -k_{di}^k \dot{V}_{si}^k / k_{si}^k = -k_{di}^k \sum_{j=1}^{r} \dot{\eta}_{ij}(t) \psi_{ij}''(x_k). \quad (7)$$

From Eq. (6), a control force vector applied on the ith link by mPZT pairs is written as

$$F_{pi} = -\sum_{k=1}^{m} k_{ai}^k k_{di}^k$$
$$\times \begin{bmatrix} (\psi_{i1}'(x_{k2}) - \psi_{i1}'(x_{k1}))\psi_{i1}''(x_k) & \cdots & (\psi_{i1}'(x_{k2}) - \psi_{i1}'(x_{k1}))\psi_{ir}''(x_k) \\ \vdots & \vdots & \vdots \\ (\psi_{ir}'(x_{k2}) - \psi_{ir}'(x_{k1}))\psi_{i1}''(x_k) & \cdots & (\psi_{ir}'(x_{k2}) - \psi_{ir}'(x_{k1}))\psi_{ir}''(x_k) \end{bmatrix}$$
$$\times \begin{pmatrix} \dot{\eta}_{i1} \\ \vdots \\ \dot{\eta}_{ir} \end{pmatrix}. \quad (8)$$

In Eq. (8), we do not need to know the values of k_{ai}^k in the practical design of the controller because $k_{ai}^k k_{di}^k$ can be regarded as a new control gain k_{Di}^k, which will be selected to damp the vibrations of the flexible link.

4. Dynamic Equations of the Manipulator System with Active Vibration Control

In this section, Lagrange's equations are used to derive the dynamic equations of the 3-PRR parallel manipulator with three flexible intermediate links bonded with PZT sensors and actuators for vibration control. Since our interest focuses on the structural vibration control of the manipulator system, the rigid-motion dynamics of the manipulator system is neither derived nor discussed here. Specifically, we adopt the Kineto-Elasto-Dynamics (KED) assumptions common to much of the literature which address structural vibration.[27] Therefore, the influence of the elastic deformation on the rigid-body motion is neglected, and the equations of motion are solved using the prescribed rigid-body motion. Thus, Lagrange's equations are formulated only for flexible generalized coordinates of the manipulator system.

To derive Lagrange's equation of the flexible parallel manipulator, we first calculate the total kinetic energy and potential energy of the manipulator system. We will analyze and incorporate generalized forces acted on flexible intermediate linkages from PZT actuators control actions.

The total kinetic energy of the manipulator system includes the kinetic energies of the sliders, intermediate links, and the platform. The kinetic energy of the three sliders is written as

$$T_S = \sum_{i=1}^{3} \frac{1}{2} m_{si} \dot{\rho}_i^2 \quad (9)$$

where m_{si} is mass of the ith slider, and $\dot{\rho}_i$ is the linear velocity of the ith slider. The kinetic energy of the three intermediate links is expressed as

$$T_L = \sum_{i=1}^{3} \frac{1}{2} \int \rho_{Ai} [\dot{\rho}_i^2 + (x\dot{\beta}_i + \dot{w}_i)^2 + 2\dot{\rho}_i (x\dot{\beta}_i + \dot{w}_i)$$
$$\times \sin(\alpha_i - \beta_i)] \, dx, \quad (10)$$

https://doi.org/10.1017/S026357470800427X Published online by Cambridge University Press

where ρ_{Ai} is mass per unit length of the ith link, $\dot{w}_i$ is the time rate of change of bending deformation of the ith intermediate link, and α_i, β_i are defined in Section 2. In Eq. (10), the model is linearized by noting that the amplitude of the vibrations is small compared to the length of the beam. Therefore, the total motion of the arbitrary point on the flexible intermediate links is the superposition of its rigid-body motion and its elastic motion. The kinetic energy of the platform is expressed as

$$T_p = \frac{1}{2}m_p\left(\dot{x}_p^2 + \dot{y}_p^2\right) + \frac{1}{2}I_p\dot{\varphi}_p^2, \tag{11}$$

where I_p is mass moment of inertia of the platform around the center point P shown in Fig. 1, m_p is the mass of the platform, $\dot{x}_p$ and $\dot{y}_p$ are the linear velocities along the X-axis and Y-axis directions, respectively, and $\dot{\varphi}_p$ is the angular velocity of platform around the point P.

Therefore, summing the kinetic energies given in Eqs. (9–11), the total kinetic energy of the system is

$$\begin{aligned} T = &\sum_{i=1}^{3}\frac{1}{2}m_{is}\dot{\rho}_i^2 + \sum_{i=1}^{3}\frac{1}{2}\int \rho_{Ai}[\dot{\rho}_i^2 + (x\dot{\beta}_i + \dot{w}_i)^2 \\ &+ 2\dot{\rho}_i(x\dot{\beta}_i + \dot{w}_i)\sin(\alpha_i - \beta_i)]\,dx \\ &+ \frac{1}{2}m_p\left(\dot{x}_p^2 + \dot{y}_p^2\right) + \frac{1}{2}I_p\dot{\varphi}_p^2. \end{aligned} \tag{12}$$

Note that since gravitational force acts along the Z-direction, perpendicular to the X–Y plane, the potential energy of the manipulator components due to gravitational force does not change during in-plane motions of the manipulator. Considering the potential energy due to deformation of the links, the potential energy of the system is given as

$$\begin{aligned} V &= \frac{1}{2}\sum_{i=1}^{3}\int E_i I_i\left(\frac{\partial^2 w_i(x)}{\partial x^2}\right)^2 dx \\ &= \frac{1}{2}\sum_{i=1}^{3}\frac{E_i}{l_i^3}\int_0^1 I_i(\xi)\sum_{j=1}^{3}\eta_{ij}^2(t)(\psi_{ij}''(\xi))^2\,d\xi \end{aligned} \tag{13}$$

where l_i is the length of the ith link, E_i elastic modulus of the ith link, and I_i second moment of area of the ith link.

From Eq. (8), the generalized forces corresponding to the generalized coordinate η_{ij} is expressed as

$$F_\eta^{ij} = \sum_{k=1}^{m} -k_{Di}^k\left(\psi_{ij}''(x_k)\sum_{j=1}^{r}\left((\psi_{ij}'(x_{k2}) - \psi_{ij}'(x_{k1})\right)\right) \tag{14}$$

Lagrange's equations for flexible generalized coordinates is given as

$$\begin{aligned} &\frac{d}{dt}\left(\frac{\partial(T-V)}{\partial\dot{\eta}_{ij}}\right) - \frac{\partial(T-V)}{\partial\eta_{ij}} = F_\eta^{ij} \\ &\quad i = 1, 2, 3 \quad j = 1, 2, \ldots, r. \end{aligned} \tag{15}$$

Substituting Eqs. (12) and (13) into (14), gives

$$\begin{aligned} &m_i\ddot{\eta}_{ij}\int_0^1 \psi_{ij}^2\,d\xi + \frac{E}{l_i^3}\eta_{ij}(t)\int(\psi_j'')^2 I_i(\xi)\,d\xi = F_\eta^{ij} \\ &- m_i\ddot{\rho}_i\sin(\alpha_i - \beta_i)\int_0^1\psi_{ij}\,d\xi - m_i l_i\ddot{\beta}_i\int_0^1\psi_{ij}\xi\,d\xi \\ &+ m_i\dot{\rho}_i\dot{\beta}_i\cos(\alpha_i - \beta_i)\int_0^1\psi_{ij}\,d\xi \end{aligned} \tag{16}$$

Equation (16) can be rewritten in matrix form as

$$M\ddot{\bar{\eta}} + K\bar{\eta} = -M_\rho\ddot{\bar{\rho}} - M_\beta\ddot{\bar{\beta}} + F_{fg} + F_{\bar{\eta}} \tag{17}$$

$$F_{\bar{\eta}} = -C\dot{\bar{\eta}} = -\begin{bmatrix} C_1 & 0 & 0 \\ 0 & C_2 & 0 \\ 0 & 0 & C_3 \end{bmatrix}\dot{\bar{\eta}} \tag{18}$$

$$\begin{aligned} C_i &= \sum_{k=1}^{m} k_{ai}^k k_{di}^k \\ &\times \begin{bmatrix} (\psi_{i1}'(x_{k2}) - \psi_{i1}'(x_{k1}))\psi_{i1}''(x_k) & \cdots & (\psi_{i1}'(x_{k2}) - \psi_{i1}'(x_{k1}))\psi_{ir}''(x_k) \\ \vdots & & \vdots \\ (\psi_{ir}'(x_{k2}) - \psi_{ir}'(x_{k1}))\psi_{i1}''(x_k) & \cdots & (\psi_{ir}'(x_{k2}) - \psi_{ir}'(x_{k1}))\psi_{ir}''(x_k) \end{bmatrix} \end{aligned} \tag{19}$$

where $m_i = \rho_{Ai}l_i$ is the modal mass of the ith intermediate link, K is the structural modal stiffness matrix, $-M_\rho\ddot{\bar{\rho}} - M_\beta\ddot{\bar{\beta}}$ reflects the effect of rigid-body motion on elastic vibration of flexible links, and F_{fg} is the modal force from the coupling between rigid-body motion and elastic motion. The detailed expressions for M, $-M_\rho$, $-M_\beta$, and F_{fg} are given in the Appendix. Parameter $F_{\bar{\eta}}$ is the modal control force vector transformed from bending moment created by PZT actuators.

Equation (17) is rewritten as

$$M\ddot{\bar{\eta}} + C\dot{\bar{\eta}} + K\bar{\eta} = -M_\rho\ddot{\bar{\rho}} - M_\beta\ddot{\bar{\beta}} + F_{fg} \tag{20}$$

It is clearly shown in Eq. (20) the essential contribution of SRF control is to introduce the damping term $C\dot{\bar{\eta}}$ into the dynamic system, and hence suppress the vibration of the flexible links.

5. Numerical Simulation and Analysis

Numerical simulations for the 3-PRR parallel manipulator with three flexible intermediate links are presented. In these simulations, a circular motion, shown in Fig. 1, is assigned as a desired trajectory for the mass center point of the moving platform with constant φ_ρ. The equations for the trajectory are $x_p = 50\cos(20\pi t) - 50$(mm), $y_p = 50\sin 20\pi t$(mm), and $\varphi_\rho = 45^\circ$. This motion is achievable with three Aerotech BM200 DC brushless servo motors (peak torque $3.5N \cdot m$) and ball screw linear guide mechanisms. Three intermediate links are modelled as aluminum alloy and have identical

https://doi.org/10.1017/S026357470800427X Published online by Cambridge University Press

Table I. Parameters of intermediate links.

Density	2.77×10^3 kg/m^3
Young's modulus	7.1×10^{10} N/m^2
Dimension	200 mm × 30 mm × 2 mm

Table II. Parameters of PZT actuators[35].

Piezoelectric d_{31}	-270×10^{-12} C/N
Young's modulus	6.3×10^{10} N/m^2
Actuator dimension	25.4 mm × 25.4 mm × 0.254 mm

geometric parameters listed in Table I. The distance between adjacent joints on the moving platform C_iC_j is100 mm. Linear guides permit a travel range of 400 mm for each slider. PZT actuators and sensors modelled here are model BM 532, manufactured by Sensor Technology. The material parameters and dimensions of PZT actuators are listed in Table II. The first three modes are to be controlled in this simulation. Considering that the midpoints of intermediate links are the nodes of the second-order mode, and to decrease the control voltages required to be applied to each PZT actuator, three PZT actuators and sensors are bonded to each of three flexible links. Three actuators and three sensors are bonded at the midpoint, quarter point, and three quarter point on each flexible link. An SRF control strategy is used to design the active vibration controller in modal space. Selection of the control gain k_{Di}^k is based on the requirement that the control voltages of PZT sensors remain less than 50 V, and the oscillatory component of the transverse deformation of the intermediate links is suppressed in less than 0.1 s. Using trial and error to satisfy these two requirements, the control gain k_{Di}^k is selected as $1.5\,N \cdot m/V^2$ in this simulation. In the strategy applied in this paper, no rigorous attempt to calculate the optimal number and locations of PZT sensors and actuators has been made, nor has an attempt to determine the optimum control gains has been made by the authors. The ideal number, location of sensors and actuators, and control gains are complex problems for multiple sensor-actuator pairs and multiple modal vibration controls. These problems can be solved by genetic algorithms or other optimization techniques.[37,38] While not the subject of this work, the control gain should be adjusted according to the collocation of PZT transducers and tuned to meet the requirement of uncertain and unmodelled dynamics by advanced control approaches, such as adaptive control, learning control, etc.

In the simulations presented here, the first three modes are selected to model the structural flexibility of intermediate links, namely $r = 3$ in Eq. (1). Therefore, flexible generalized coordinates in Eq. (17) are $\bar{\eta} = [\eta_{11}\ \eta_{12}\ \eta_{13}\ \eta_{21}\ \eta_{22}\ \eta_{23}\ \eta_{31}\ \eta_{32}\ \eta_{33}]^T$. The rigid-body motion of sliders and intermediate linkages is derived from the given motion of the moving platform by solving inverse kinematics of the parallel manipulator. Substituting the rigid-body motion into Eq. (17), and with initial conditions $\bar{\eta} = 0_{9\times1}$, $\dot{\bar{\eta}} = 0_{9\times1}$, Eq. (17) are solved for the first two periods (50 ms for a period) of the moving platform using MATLAB ODEs solver ode113 based on a variable order Adams–Bashforth–Moulton method.[29]

Figure 3 presents elastodynamic response of the midpoint of the first intermediate link with and without control

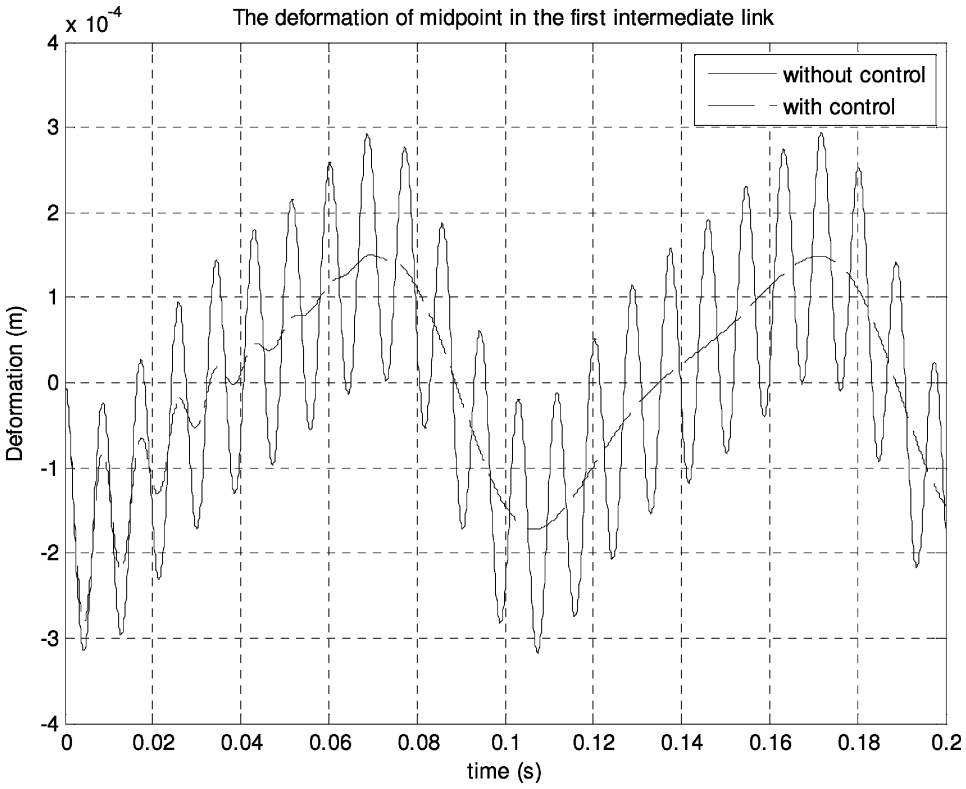


Fig. 3. The deformation at the midpoint of intermediate links.

https://doi.org/10.1017/S026357470800427X Published online by Cambridge University Press

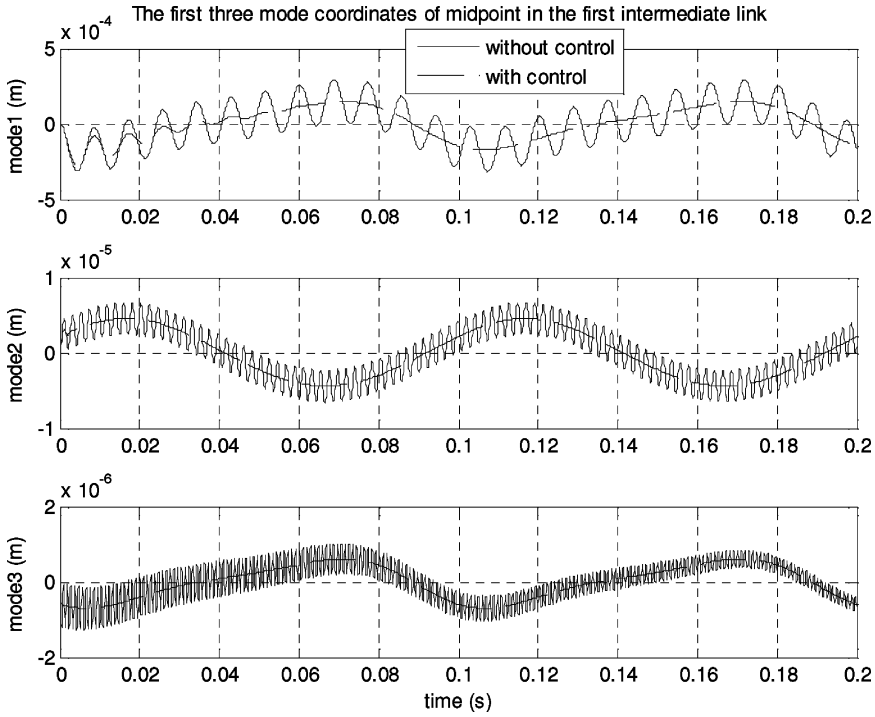


Fig. 4. The first three vibration modes of the 1st intermediate link.

action. The elastodynamic response is the superposition of structural free vibration and substantially lower frequency deflection caused by inertial forces and coupling forces. It is clearly illustrated, in this figure, that the magnitude of the midpoint deflection due to free vibration was substantially suppressed by employing PZT actuators. Figure 4 further reveals that the first three modes of vibrations are effectively reduced, and the second and third mode of vibrations are reduced substantially more than the first mode of vibration. It is interesting to observe from these figures that the deflection caused by structural free vibration was completely eliminated by the imposed control voltages, shown in Fig. 5, while the deflection caused by the inertial forces and coupling forces remained. This phenomenon is confirmed by frequency analysis of flexible intermediate links and the spectral analysis of the elastodynamic response, with and without PZT actuator control inputs, given in Figs. 6 and 7. The power spectral density for the vibration response illustrates in Figure 6 that the vibration energy is greatest at the frequencies of 10 Hz, 20 Hz, and 116.4 Hz. From Eq. (17), the vibration response includes free vibration and forced vibration from inertial and coupling forces. The jth mode vibration frequencies of the ith intermediate links can be written as $\omega_{ij} = (j\pi/l_i)^2\sqrt{EI_i/\rho A_i}$. Therefore, the first three mode frequencies are calculated to be 116.4 Hz, 465.6 Hz, and 1047.5 Hz. This implies that in Fig. 6, the vibration with the frequency of 116.4 Hz is a free vibration, and the vibrations with frequencies of 10 Hz and 20 Hz are forced vibrations. Figure 8 shows the time history of the inertial and coupling forces applied on the first intermediate link expressed in the first mode space, where F_1 corresponds to $-M_\rho\ddot{\tilde{\rho}}$, F_2 corresponds to $-M_\beta\ddot{\tilde{\beta}}$, and F_3 corresponds to

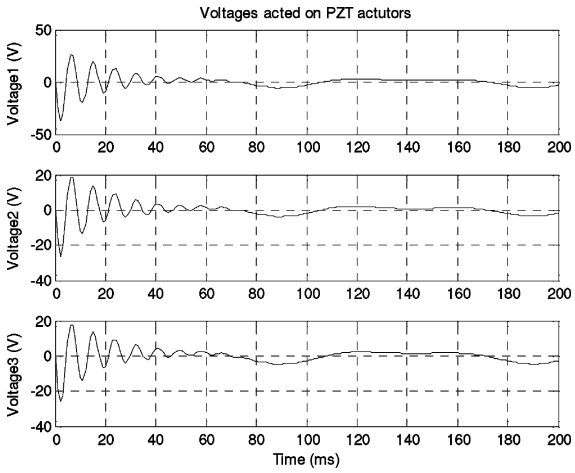


Fig. 5. Control voltages on PZT actuators of the 1st link.

F_{fg}. Frequency spectral analyses for the inertial and coupling forces are performed using FFT. Analysis results show that frequencies of these forces are 10, 20 and 30 Hz, and the power density of 10 Hz exhibits the largest peak, which is consistent with the frequency spectra of the vibration response, as shown in Fig. 6. Comparing Figs. 6 and 7, it is clearly shown that the vibration with frequency of 116.4 Hz was completely suppressed, but the vibrations with frequencies of 10 and 20 Hz were not reduced. These results are consistent with the results given in Figs. 3 and 4.

Figure 4 reveals that the amplitude of the first mode vibration of the first intermediate link is two orders of

https://doi.org/10.1017/S026357470800427X Published online by Cambridge University Press

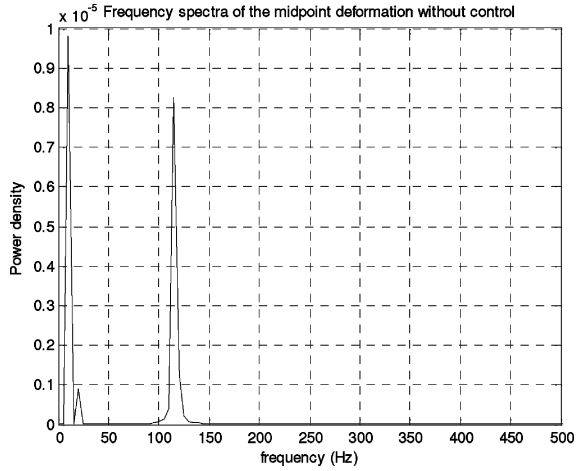


Fig. 6. Frequency spectra of vibration response without control.

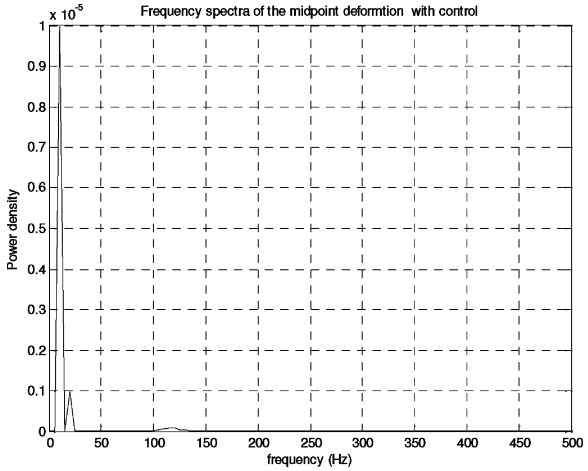


Fig. 7. Frequency spectra of vibration response with control.

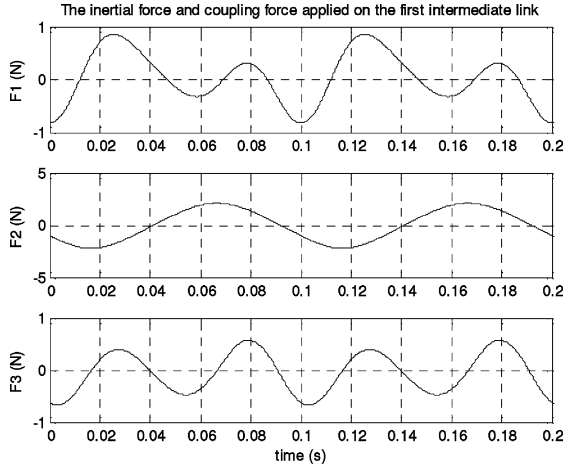


Fig.8. Inertial and coupling forces of the 1st mode.

magnitudes larger than the amplitude of the second mode vibration. Therefore, the dynamic responses contributed by those neglected modes are rather small. The effect of neglected modes can be addressed by adopting adaptive and learning control technologies, which is the subject of our ongoing research effort. It is obvious that the first mode is sufficiently accurate to describe the vibration of the flexible intermediate link. Therefore, it is reasonable to reduce the number of modelled vibration modes to small finite number, which can be further reduced for real-time control.

6. Conclusion and Continuing Efforts

This paper has presented simulation results of the active vibration control of elastodynamic response of the moving 3-PRR parallel manipulators with three flexible intermediate links bonded with multiple PZT actuators and sensors. An active PZT actuator and senor controller has been designed in modal space based on strain rate feedback control. Incorporated with control forces from PZT actuators, a procedure for the generation of dynamic equations for a 3-PRR parallel manipulator with three flexible intermediate links has been addressed based on the assumed mode method. The mode shape functions are selected by modelling intermediate links as Euler–Bernoulli beams with pinned-pinned boundary conditions. A reduced order and linearized model has been developed to decrease the calculation burden, and therefore the model is feasible for real-time control. Numerical simulations are performed, and simulation results show that the deflections caused by structural free vibration were almost completely eliminated by the imposed control voltages, but the deflections caused by the inertial forces and coupling forces were not reduced. The unreduced deformations may be suppressed using other control strategies such as controlling the joint torque, introducing additional microprocessor controlled actuators to the original mechanisms, etc.

In the forthcoming work, experimental investigation will be performed to verify the strain rate feedback vibration control strategy. Advanced control methods, such as adaptive control and learning control, will also be developed to compensate the unmodelled dynamics of the flexible parallel manipulator system in our future research work.

References

1. R. C. Winfrey, "Elastic link mechanism dynamics," *ASME J. Eng. Ind.* **93**, 268–272 (1971).
2. W. Sunada and S. Dubowsky, "The application of the finite element methods to the dynamic analysis of flexible spatial and co-planar linkage systems," *ASME J. Mech. Des.* **103**(3), 643–651 (1981).
3. W. J. Book, "Recursive Lagrangian dynamics of fexible manipulator arms," *Int. J. Robot Res.* **3**(3), 87–101 (1984).
4. H. Asada, Z.-D. Ma and H. Tokumaru, "Inverse dynamics of flexible robot arms: Modeling and computation for trajectory control," *ASME. J. Dyn. Syst. Meas. Control* **112**, 177–185 (1990).

https://doi.org/10.1017/S026357470800427X Published online by Cambridge University Press

5. A. A. Shabana, "Flexible multibody dynamics: review of past and recent developments," *Multibody Syst. Dyn.* **1**, 189–222 (1997).
6. M. Giovagnoni, "Dynamics of Flexible Closed-chain Manipulator," *ASME Design Technical Conference* 69-2, Scottsdale, Arizona, USA (1992) pp. 483–490.
7. J. D. Lee and Z. Geng, "Dynamic model of a flexible Stewart platform," *Comput. Struct.* **48**(3), 367–374 (1993).
8. Z. Zhou, J. Xi and C. K. Mechefske, "Modeling of a fully flexible 3PRS manipulator for vibration analsysis," *J Mech. Des.* **128**, 403–412 (2006).
9. X., Wang, and J. K. Mills, "FEM dynamic model for active vibration control of flexible linkages and its application to a planar parallel manipulator," *Appl Acous.* **66**, 1151–1161 (2005).
10. Xuping Zhang, J, K. Mills and W. L. Cleghorn, "Dynamic modeling and experimental validation of a 3-PRR parallel manipulator with flexible intermediate link," *J. Intell. Robot. Syst.* **50**, 323–340 (2007).
11. X. M. Zhang, Y. W. Shen, H. Z. Liu and W. Q. Cao, "Optimal design of flexible mechanisms with frequency constraints," *Mech. Mach. Theory* **30**(1), 131–139 (1995).
12. W. L. Cleghorn, F. G. Fenton and B. Tabarrok, "Optimal design of high-speed flexible mechanisms," *Mech. Mach.* Theory **16**, 339–406 (1981).
13. E. H. El-Dannah and S. H. Farghaly, "Vibratory response of a sandwich link in a high-speed mechanism," *Mech. Mach.* Theory **28**, 447–457 (1993).
14. C. Sisemore, A. Smaili and R. Houghton, "Passive damping of flexible mechanism systems: Experimental and finite element investigations," In: *The 10th World Congress on the Theory of Machines and Mechanisms*, Oulu, Finland (Jun. 20–24, 1999), vol. 5, pp. 2140–2145.
15. A. Ghazavi, F. Gardanine and N. G. Chalhout, "Dynamic analysis of a composite material flexible robot arm," *Comput. Struct.* **49**, 315–325 (1993).
16. C. K. Sung and B. S. Thompson, "Material selection: An important parameter in the design of high-speed linkages," *Mech. Mach.* Theory **19**, 389–396 (1984).
17. H. Ulbrich and H. V. Stein, "A combined feedforward-feedback control strategy for improving the dynamics of a flexible mechanism," *Multibody Syst. Dyn. Theory* **7**, 229–248 (2002).
18. N. C. Singer and W. P. Seering, "Using a Causal Shaping Techniques to Reduce Robot Vibrations", *Proceedings of IEEE International Conference on Robotics and Automation*, Philadelphia (1988) pp. 1434–1439.
19. B. Siciliano and W. Book, "A singular perturbation approach to control of lightweight flexible manipulators", *Int. J. Robot. Res.* **7**(4), 79–90 (1988).
20. S. F. Asokanthan and M. Gu, "Distributed Control of Flexible Structure: Theory and Experiment," *Proceedings of Asia-Pacific Control Conference*, Brooklyn, New York, USA (1995) pp. 539–553.
21. T. Bailey and J. J. Hubbard, "Distributed piezoelectric-polymer active vibration control of a cantilever beam," *J. Guid. Control Dyn.* **9**(5), 605–611 (1985).
22. Z. Li and P. M. Bainum, "Vibration control of flexible spacecraft integrating a momentum exchange controller and a distributed piezoelectric actuator," *J. Sound Vib.* **177**(4), 539–553 (1994).
23. S. B. Choi and H. C. Shin, "A hybrid actuator scheme for robust position control of a flexible single-link manipulator," *J. Robot. Syst.* **13**(6), 359–370 (1996).
24. E. F. Crawley and D. Luis , "Use of piezoelectric actuators as elements of intelligent structures," *AIAA J.* **25**(10), 1373–1385 (1987).
25. F. Khorrami, I. Zeinoun and E. Tome, "Experimental Results on Active Control of Flexible-link Manipulators with Embedded Piezoceramics," *Proceedings of IEEE International Conference Robotics and Automation*, Atlanta, GA, USA (1993) pp. 222–227.
26. G. Song, S. P. Schmidt and B. N. Agrawal, "Active vibration suppression of a flexible structure using smart material and modular control patch," *Proc. Inst. Mech. Eng.* **214**, 217–229 (2000).
27. C. K. Sung and Y. C. Chen, "Vibration control of the elastodynamic response of high-speed flexible linkage mechanisms," *ASME J. Vib. Acoust.* **113**(1), 14–21 (1991).
28. D. Sun, J. K. Mills, J. Shan and S.K. Tso, "A PZT actuator control of a single-link flexible manipulator based on linear velocity feedback and actuator placement," *Mechatronics* **14**, 381–401 (2004).
29. "Solve initial value problems for ordinary differential equations (ODEs)," MATLAB Function Reference, The Math Works, Inc. 1994-2005.
30. S. Staicu, D. Zhang and R. Rugescu, "Dynamic modelling of 3-DOF parallel manipulator using recursive matrix relations," *Robotica* **24**, 125–130 (2006).
31. B. Kang, B. Yeung and J. K. Mills, "Two-time scale controller design for a high speed planar parallel manipulator with structural flexibility," *Robotica* **20**, 519–528 (2002).
32. L. Meirovitch and H. Baruh, "Optimal control of damped flexible gyroscopic systems," *J. Guid. Control* **4**, 157–163, (1981).
33. A. Baz and S. Poh, "Performance of an active control system with piezoelectric actuators," *J. Sound Vib.* **126**(2), 327–343 (1988).
34. S. P. Singh, H. S. Pruthi and V. P. Agarwal, "Efficient modal control strategies for active control of vibrations," *J. Sound Vib.* **262**, 563–575 (2003).
35. Product Catalogue, Sensor Technology Ltd., Collingwood, Ontario, Canada, 2007.
36. C. M. Gosselin, S. Lemieux and J.-P. Merlet,"A New Architecture of Planar Three-Degree of Freedom Parallel Manipulator," *Proceedings of the IEEE International Conference on Robotics and Automation*, Minneapolis, Minnesota, (1996) pp. 3738–3743.
37. X. J. Yan and L. H. Yam, "Optimal design of number and locations of actuators in active vibration control of a space truss," *Smart Mater. Stuct.* **11**, 496–593 (2002).
38. M. M. Abdullah, "Optimal locations and gains of feedback controllers at discrete locations," *AIAA J.* **36**(11), pp. 2109–2116 (1998).

https://doi.org/10.1017/S026357470800427X Published online by Cambridge University Press

Appendix

$$M = \begin{bmatrix} \hat{M}_1 & 0 & 0 \\ 0 & \hat{M}_2 & 0 \\ 0 & 0 & \hat{M}_3 \end{bmatrix} \in R^{3r\times 3r} \quad \hat{M}_i = m_i \begin{bmatrix} \int \psi_{i1}^2\, d\xi & \cdots & 0 \\ \vdots & \cdots & \vdots \\ 0 & \cdots & {}_i\int \psi_{ir}^2\, d\xi \end{bmatrix} \in R^{r\times r} \quad i = 1, 2, 3$$

$$K = \begin{bmatrix} \hat{K}_1 & 0 & 0 \\ 0 & \hat{K}_2 & 0 \\ 0 & 0 & \hat{K}_3 \end{bmatrix} \in R^{3r\times 3r} \quad \hat{K}_i = \frac{E_i}{l_i^3} \begin{bmatrix} \int I_i(\xi)\psi_{i1}''^2\, d\xi & \cdots & 0 \\ \vdots & \cdots & \vdots \\ 0 & \cdots & \int I_i(\xi)\psi_{ir}''^2\, d\xi \end{bmatrix} \in R^{r\times r}$$

$$M_\rho = \begin{bmatrix} m_1 s_1 \int \psi_{11}\, d\xi & \cdots & m_1 s_1 \int \psi_{1r}\, d\xi & 0 & \cdots & 0 & 0 & \cdots & 0 \\ 0 & \cdots & 0 & m_2 s_2 \int \psi_{21}\, d\xi & \cdots & m_2 s_2 \int \psi_{2r}\, d\xi & 0 & \cdots & 0 \\ 0 & \cdots & 0 & 0 & \cdots & 0 & m_3 s_3 \int \psi_{31}\, d\xi & \cdots & m_3 s_3 \int \psi_{3r}\, d\xi \end{bmatrix}^T$$

$$M_\beta = \begin{bmatrix} m_1 l_1 \int \psi_{11}\, d\xi & \cdots & m_1 l_1 \int \psi_{1r}\, d\xi & 0 & \cdots & 0 & 0 & \cdots & 0 \\ 0 & \cdots & 0 & m_2 l_2 \int \psi_{21}\, d\xi & \cdots & m_2 l_2 \int \psi_{2r}\, d\xi & 0 & \cdots & 0 \\ 0 & \cdots & 0 & 0 & \cdots & 0 & m_3 l_3 \int \psi_{31}\, d\xi & \cdots & m_3 l_3 \int \psi_{3r}\, d\xi \end{bmatrix}^T$$

$$F_{fg} = \begin{bmatrix} m_1 c_1 \dot{\rho}_1 \dot{\beta}_1 \int \psi_{11} d\xi \\ \vdots \\ m_1 c_1 \dot{\rho}_1 \dot{\beta}_1 \int \psi_{1r} d\xi \\ m_2 c_2 \dot{\rho}_2 \dot{\beta}_2 \int \psi_{21} d\xi \\ \vdots \\ m_2 c_2 \dot{\rho}_2 \dot{\beta}_2 \int \psi_{2r} d\xi \\ m_3 c_3 \dot{\rho}_3 \dot{\beta}_3 \int \psi_{31} d\xi \\ \vdots \\ m_3 c_3 \dot{\rho}_3 \dot{\beta}_3 \int \psi_{3r} d\xi \end{bmatrix}$$

where $s_i = \sin(\alpha_i - \beta_i)$ and $c_i = \cos(\alpha_i - \beta_i)$.

https://doi.org/10.1017/S026357470800427X Published online by Cambridge University Press